

Comparison on the Microstructure and Wear Behaviour of Flame Sprayed Ni-Based Alloy Coatings Remelted by Flame and Induction

Bunv Liang¹ · Zhenyu Zhang¹ · Hongjian Guo²

Received: 27 November 2015 / Accepted: 25 November 2016 / Published online: 8 December 2016
© The Indian Institute of Metals - IIM 2016

Abstract This paper analyses the influence of remelting process on the microstructure characteristics and wear behavior of NiCrBSi alloy coatings. Two different remelting processes are investigated to obtain improvement in properties: flame spraying combined with flame remelting and flame spraying combined with induction remelting. A comparison of the microstructure and the tribological behavior is presented. A field-emission gun scanning electron microscope, energy dispersive X-ray microanalysis and X-ray diffraction analysis have been used to observe the microstructure characteristics of the coatings. The results reveal significant differences in the morphology, distribution, size and percentage of the phases of both coatings. The induction remelting technique results in higher Vickers hardness, excellent wear resistance and good remelting quality.

Keywords NiCrBSi alloy · Flame spray · Induction remelting · Microstructure · Wear behavior

1 Introduction

Thermal spray is widely used in industry because of its versatile processes and economical options [1–3]. In thermal spraying, the coating material is fed to a heating zone

in order to melt them, followed by the acceleration of the molten material leading to surface impacts, where rapid solidification and modified coating build-up occurs [3–5]. Flame spray is one of the most popular and economical techniques among thermal sprays and can be used for a wide range of materials. However, flame spray coatings have high porosity, forming oxide interlayers, and the lack of a mechanical bond between the coating and the substrate leads to the poor adherence to the substrate [6–10]. Therefore, subsequent remelting is necessary to reduce porosity and create a metallurgical bond between the coating and substrate materials, which enhances the bond strength of the coating [11–15].

Different methods are applied to melt flame sprayed coatings; the flame remelting process has been the most commonly used method for several decades because of its versatile and economical features. Nevertheless, it is not easy to precisely control flame remelting process, and satisfactory results cannot be guaranteed [16–18]. Therefore, the induction remelting technique is used in the processing of flame sprayed Ni-based alloy coatings, which helps to attain the required temperature via an applied magnetic field over a short interaction time [19–21]. Moreover, the induction remelting technique has the advantages of high melting speeds, dramatic energy savings and a clear environment [18, 21]. Because of these advantages, this paper evaluates the induction remelting technique as an alternative to the flame remelting method. Because the process parameters can be easily controlled using the induction remelting technique, the quality of the coatings and the mechanical and wear properties can be improved. The aim of this work is to compare the two remelting processes (flame and induction remelting) based on the microstructure and wear behavior of flame sprayed Ni-based alloy coatings to establish relations between the

✉ Zhenyu Zhang
zhzhyu428@163.com

¹ Material Engineering Department, Lanzhou Institute of Technology, Lanzhou, Gansu 730050, China

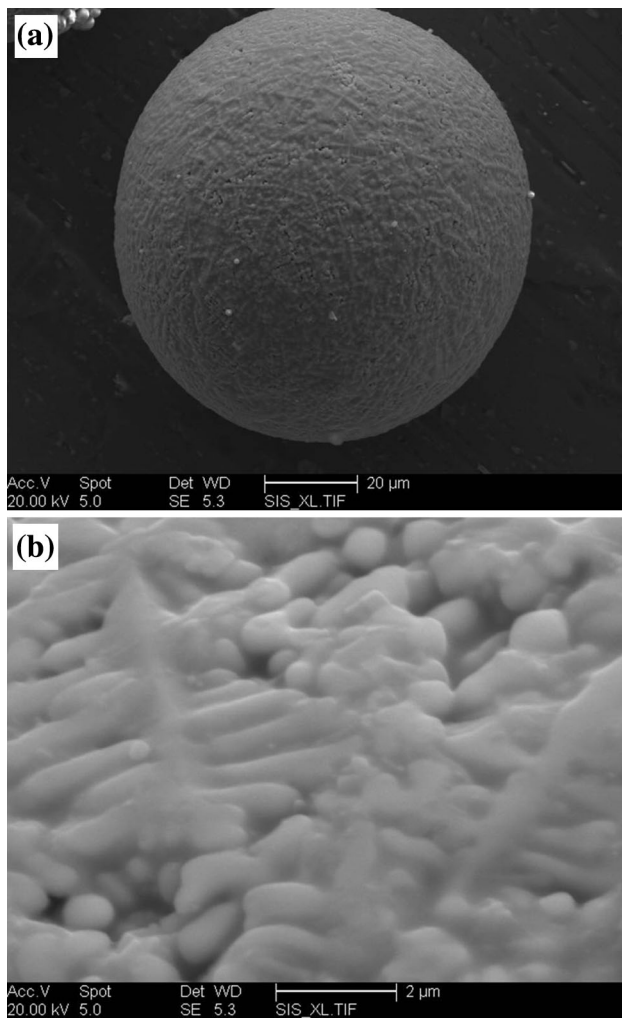
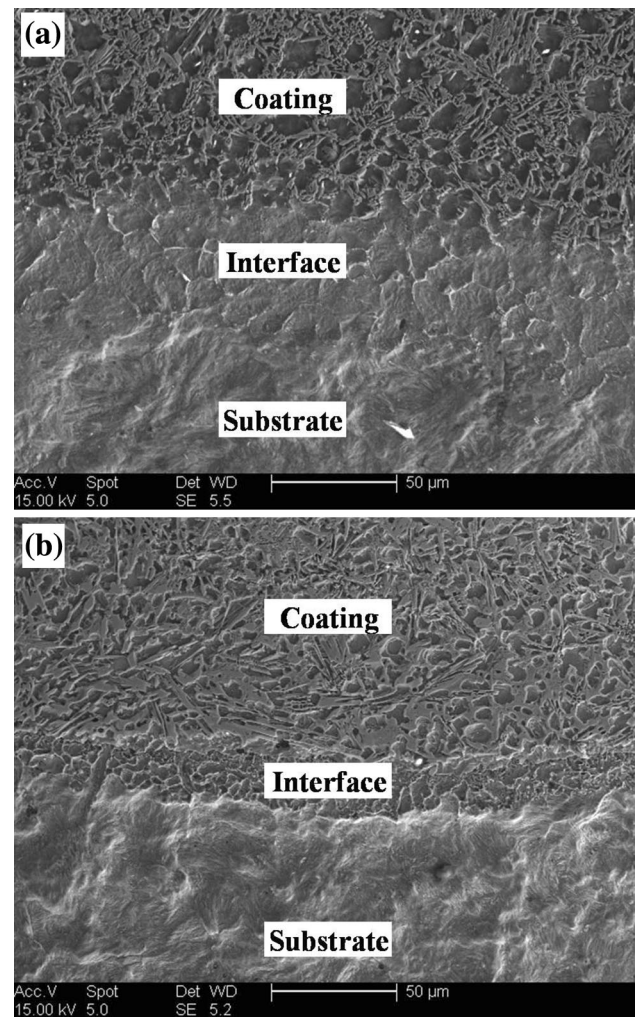
² State Key Laboratory of Solid Lubrication, Lanzhou Institute of Chemical Physics, Chinese Academy of Sciences, Lanzhou 730050, China

Table 1 Chemical composition of alloys

Weight (%)	C	Ni	Cr	Fe	B	Si	P	S	Mn
Ni-based alloy	0.8	Bal.	16	4	3.5	3.8	–	–	–
1045 carbon steel	0.15	–	–	Bal.	–	0.27	0.32	0.32	0.45

Table 2 Chemical composition of SAE52100 steel (in wt.%)

Weight (%)	C	Cr	Mn	Si	Fe
SAE52100	0.95–1.05	1.30–1.65	0.2–0.4	0.15–0.35	Bal.

**Fig. 1** Powder morphology of the Ni-based alloy obtained by gas atomization: **a** FEGSEM image of the atomization powder; **b** details of the dendritic crystals**Fig. 2** Microstructure of the cross sectional morphology of the coatings: **a** flame-remelted coatings; **b** induction-remelted coatings

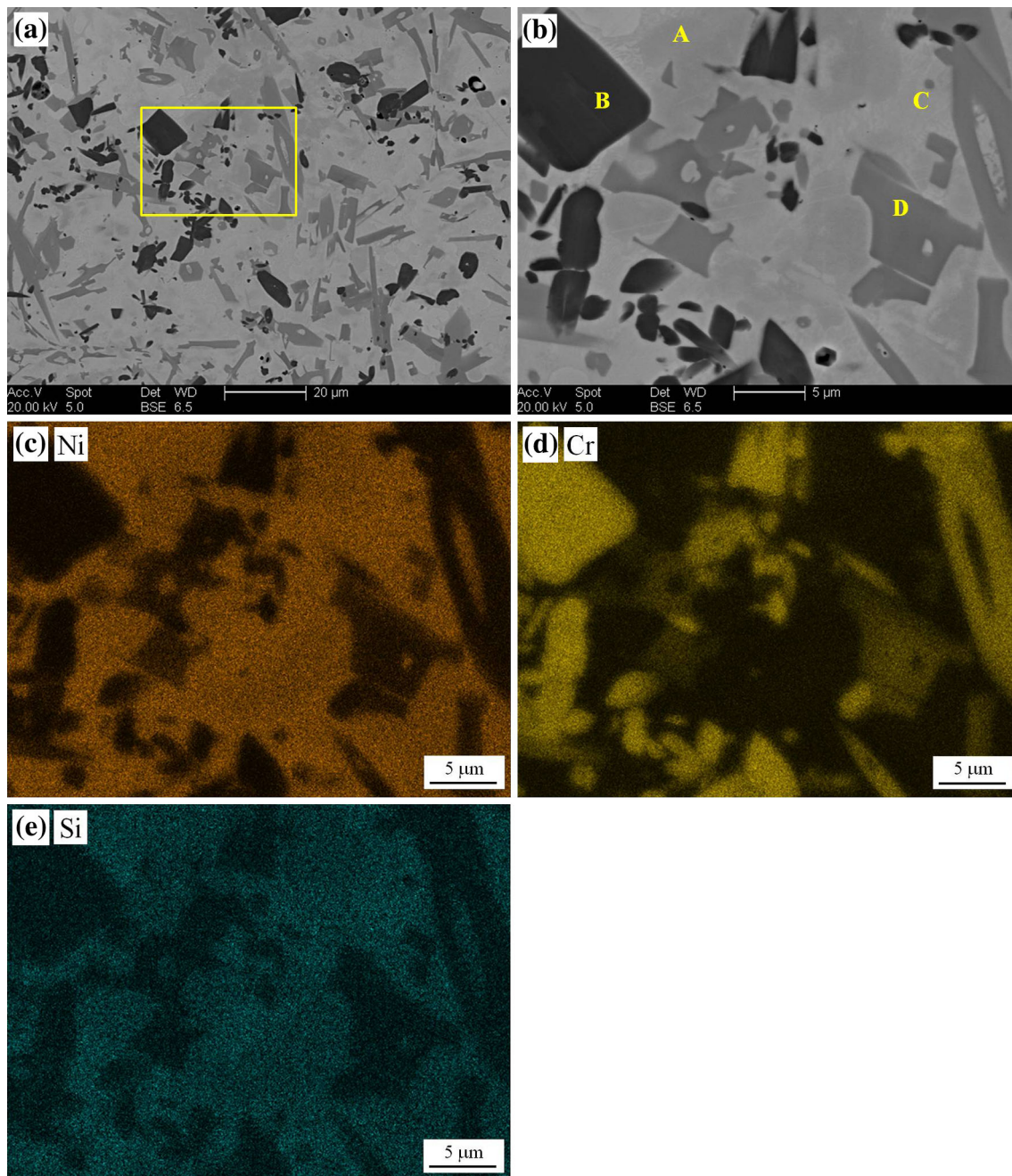


Fig. 3 BSI and EDS mapping images of the Ni-based alloy coatings remelted by flame: **a** BSI morphology; **b** high magnification image of the marked area; **c** the elemental map of Ni; **d** the elemental map of Cr; **e** the elemental map of Si

wear behavior and microstructure of the coatings for the different remelting processes.

2 Experimental Details

Commercial NiCrBSi alloy powders were used as the coating material. The shape of the powder particles were spherical, with an average diameter of 65 μm ; and a

melting point of 1020 $^{\circ}\text{C}$. The substrate material was 1045 carbon steel (Table 1).

The surface of the substrate was cleaned and grit blasted with Al_2O_3 grade 24 before spraying. A SPH-7/h gun (China) was used to perform flame spraying at a pressure of 400 kPa for oxygen and 55 kPa for acetylene. The oxygen and acetylene flow rates were 1.2 and 0.85 m^3/h , respectively. The optimal spraying distance was 150–180 mm. After spraying, each coating was remelted by a SP-C-4

flame melting gun that applied an oxy-acetylene flame onto the coating until the melting point was reached. The flame spraying being a manual process, the quality of the coatings depended on the ability and experience of the operators.

UP-100-10 (USA) mid-frequency inductive equipment was also used to remelt the flame sprayed coatings. The coatings were completely melted by continuous heating via a close-up eddy current generated from the magnetic field. The induction remelting process was completed at an induction frequency of 10 Hz and a power of 100 kW.

A field-emission gun scanning electron microscope (FEGSEM) equipped with EDS was used to analyze the microstructure of the coatings. Specimens for microstructural analysis were polished with fine diamond paste and then etched in a mixture composed of 10 ml of HNO₃ and 30 ml of HCl. The phase structure of the coatings was determined using an X'Pert PRO X-ray diffraction (XRD) instrument. An MH-5-VM tester with a load of 4.9 N measured the microhardness along the cross-sectional depth.

Tribological evaluation of the coatings was performed using a ball-on-disc tribometer (an Optimol SRV oscillating friction and wear tester). Dry sliding wear tests at a room temperature of approximately 26 °C and relative humidity of approximately 55% were performed. The coated discs were tested against SAE52100 steel bars with a diameter of 9.53 mm and a hardness of HRC 62–63; the chemical composition of SAE52100 steel is presented in Table 2. The tests were performed under the following conditions: an oscillating amplitude of 1 mm, normal loads of 20–100 N, frequency of 10–50 Hz, and duration of 20 min. Before the tests were performed, the discs were machined into Ø 24 mm × 7 mm polished with 500-grit emery paper, cleaned in an acetone ultrasonic bath for 20 min, and then dried in hot air. The morphologies of the worn surface of the samples were examined using the FEGSEM.

3 Results and Discussion

3.1 Microstructure Characterization

Figure 1 shows the FEGSEM observation of the NiCrBSi alloy powder. The powder is found to exhibit a dendritic structure resulting from the rapid solidification condition due to gas atomization, and the powder has fine spherical grains. In particular, very fine dendritic crystals are found in the high magnification micrographs (Fig. 1b). Figure 2 shows the cross sectional morphology of the coatings. A metallurgical bond area between the coating and substrate is observed. Fig. 3 shows the back-scattered electron image

and the EDS mapping images of the flame spray and flame remelted NiCrBSi alloy coatings. A high magnification is required to analyze the constituents resulting from the flame remelting technique, as shown in Fig. 3b–e. The microstructure consists of structures of different morphologies that are heterogeneously distributed across the metallic matrix. EDS analysis of the higher magnification images indicates that the matrix (marked A) is rich in Ni and Si and is poor in Cr. The dark blocky phase (marked B) contains a higher concentration of Cr. The eutectic structures (marked C) are rich in Ni and Si and are poor in Cr. The grey phase (marked D) exhibits several morphologies: blocky, irregular and needle-like structures; this phase

Table 3 EDS analysis of the Ni-based alloy coatings remelted by flame (in wt.%)

Region	C	Ni	Cr	Fe	B	Si
A	0.69	75.15	9.35	11.05	2.30	1.46
B	1.73	4.86	69.75	8.07	14.53	1.06
C	0.91	80.4	4.54	3.7	3.02	7.43
D	9.85	18.73	59.15	9.39	1.03	1.85

Table 4 EDS analysis of the Ni-based alloy coatings remelted by induction (in wt.%)

Region	C	Ni	Cr	Fe	B	Si
A	1.09	69.65	9.15	8.51	9.52	2.08
B	2.13	1.86	75.86	6.27	13.83	0.05
C	0.33	78.23	3.57	6.6	3.02	8.25
D	12.42	7.58	69.46	8.39	1.08	1.07

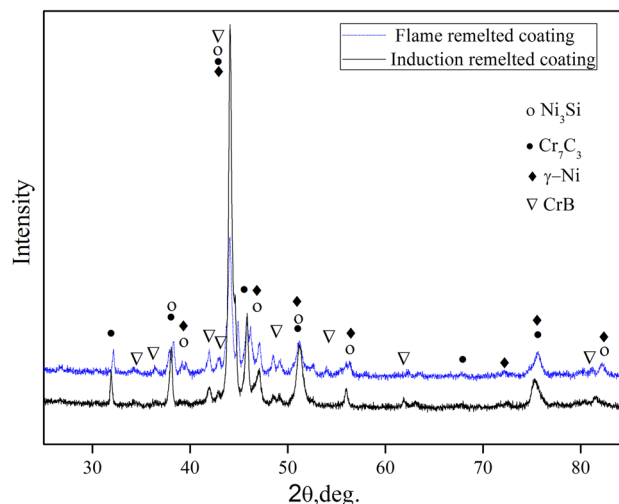


Fig. 4 XRD pattern of the coatings remelted by induction and flame

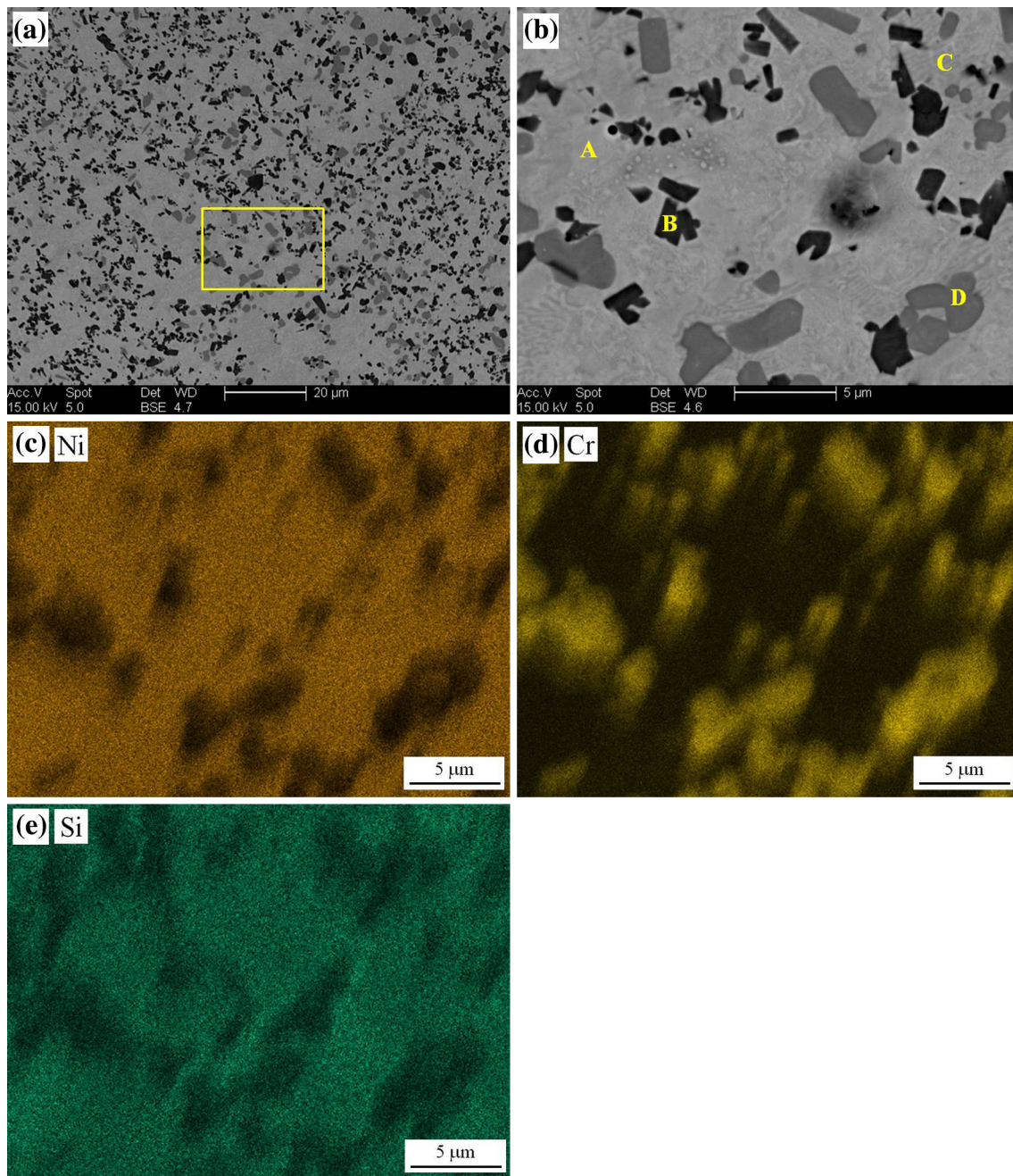


Fig. 5 BSI and EDS mapping images of the Ni-based alloy coatings remelted by induction heating: **a** BSI morphology; **b** high magnification image of the *marked area*; **c** the elemental map of Ni; **d** the elemental map of Cr; **e** the elemental map of Si

mainly contains Cr. The quantitative chemical analysis of the phases are shown in Tables 3 and 4. The X-ray diffraction pattern of the flame remelted coatings is shown in Fig. 4. The pattern reveals that the microstructure of the flame remelted coatings consists of γ -Ni, CrB, Ni_3Si and Cr_7C_3 . Based on previous research results using XRD and EDS or TEM [5, 8, 12, 13, 15], the results from the XRD, EDS and FEGSEM measurements strongly suggest the following: the matrix mainly consists of γ -Ni, the dark

blocky phase is CrB type chromium boride, and the grey phase is Cr_7C_3 chromium carbide. The eutectic phase mainly consists of γ -Ni and Ni_3Si .

A similar microstructure is also observed in the coatings obtained by the induction remelting process (as shown in Fig. 5). The details of the coatings and the EDS analysis are shown in Fig. 5b–e. Quite similar phases compared to the coatings remelted by flame are shown in Fig. 4. The particle size of the dark blocky CrB phase is found to be in

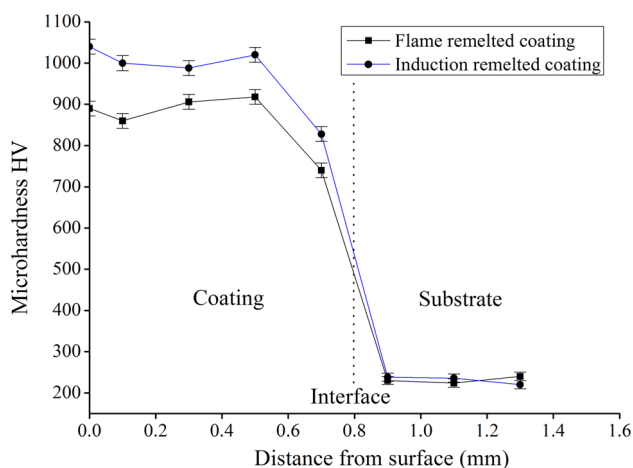


Fig. 6 Microhardness profile for the induction and flame-remelted coatings

the range from 1 to 3 μm , while the particle size of the dark blocky CrB phase in the flame remelted coatings is found to be in the range from 3 to 10 μm . In addition, the size of grey Cr_7C_3 is also obviously different: ranging from 3 to 5 μm in flame remelted coatings and ranging from 5 to 20 μm in induction remelted coatings. Furthermore, substantial differences are found in the shape, distribution and morphology between the two types of coatings.

3.2 Microhardness Distribution

Figure 6 shows the microhardness distribution of the coatings as a function of the distance from the surface to the substrate. A graded distribution increasing from the interface to the upper side of the coatings is found. Three distinct regions are observed in the hardness profile. The microhardness values of the induction remelted coatings are higher than those of the coatings remelted by flame process. The improvement in the hardness of the coatings using the induction remelting method may be due to the uniformly distributed microstructure. In addition, the difference in the microhardness of the coatings is due to the dilution between the substrate and the coating [18]. In the induction remelted coatings, the dilution can be limited during short-time remelting via the applied magnetic field, which is beneficial for the hardness of the coatings [18].

3.3 Sliding Wear Behaviors

Figure 7 shows the results from the wear testing. The wear rate, as a function of the sliding speed, is linear for the coatings remelted by flame and induction (as shown in Fig. 7a), and the wear rate increases with increasing sliding speed. The wear rate of the coatings remelted by induction is observed to be slightly lower than that of the coatings

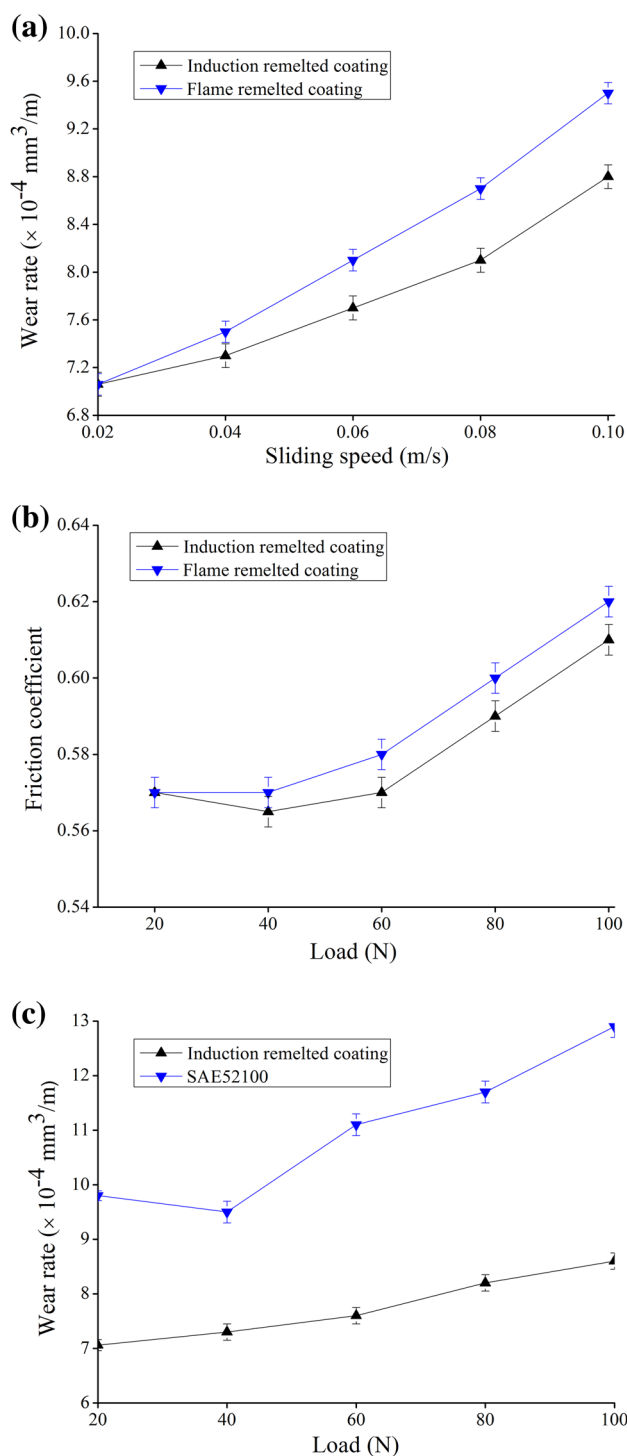


Fig. 7 Tribological properties of the coatings at a duration of 20 min: **a** variation of the wear rate of specimen at 40 N with sliding speed; **b** the friction coefficient at a sliding speed of 0.05 m/s with a load; **c** the variation of the wear rate of the specimen at a sliding speed of 0.05 m/s with a load

remelted by flame. The friction coefficient has also been measured for each test, and its average value has been calculated; the friction coefficient values increase slightly

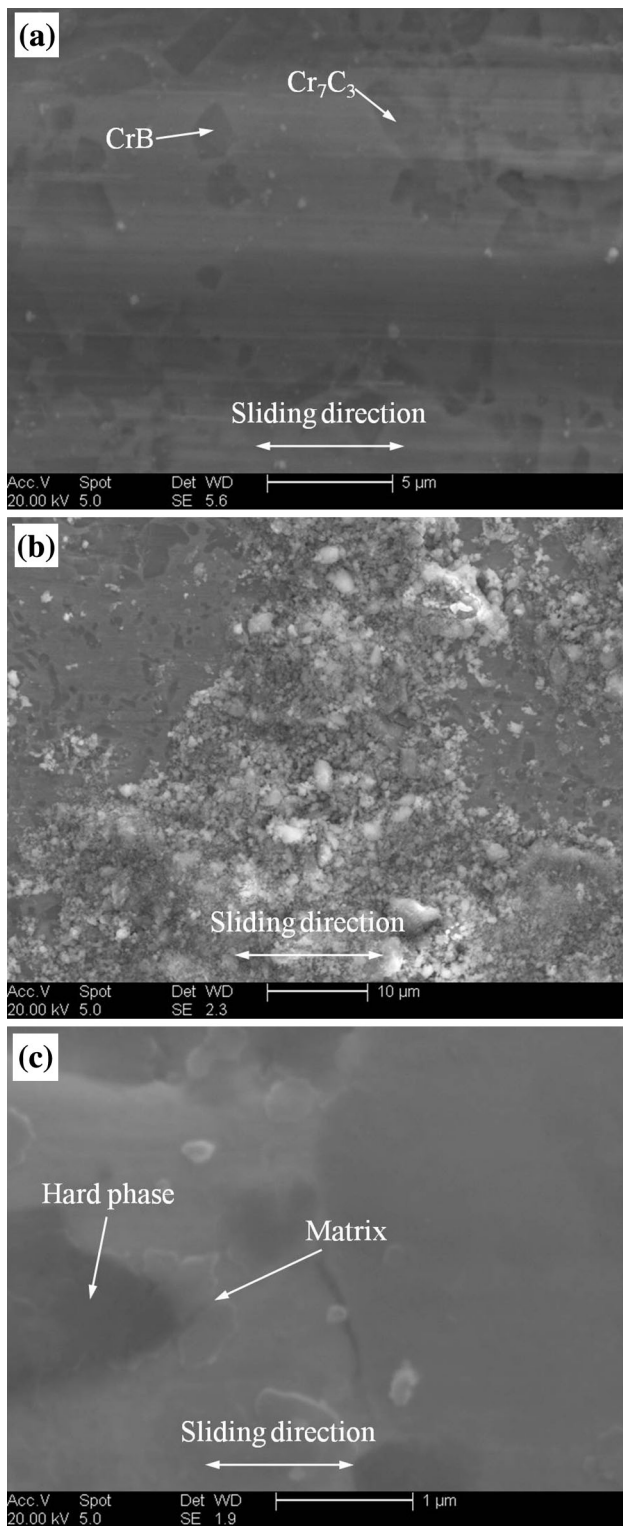


Fig. 8 FEGSEM morphologies of the worn surfaces of the Ni-based alloy coatings remelted by induction after a sliding duration of 20 min at a linear speed of 0.05 m/s and normal loads of: **a** $P = 40$ N, $V = 0.05$ m/s; **b** $P = 100$ N, $V = 1.0$ m/s; **c** $P = 50$ N, $V = 0.06$ m/s

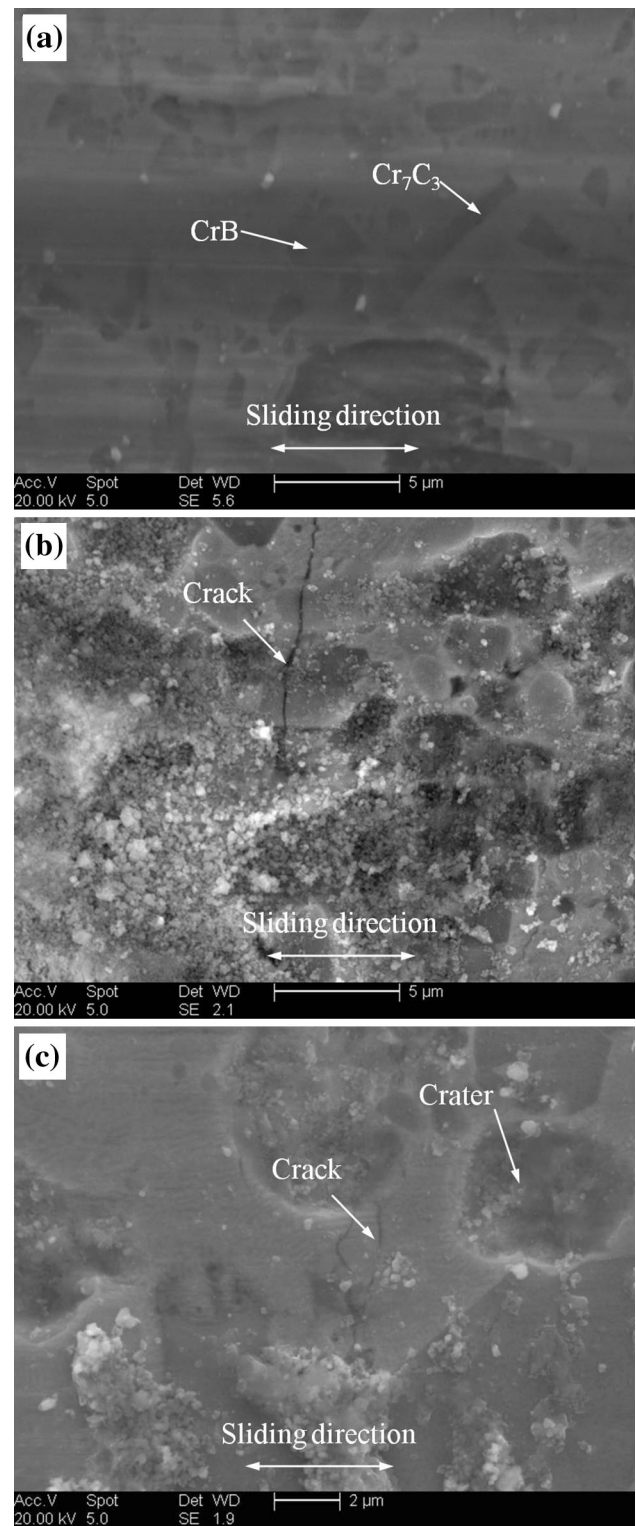


Fig. 9 FEGSEM morphologies of the worn surfaces of Ni-based alloy coatings remelted via flame after a sliding duration of 20 min at a linear speed of 0.05 m/s and normal loads of: **a** $P = 40$ N, $V = 0.05$ m/s; **b** $P = 100$ N, $V = 1.0$ m/s; **c** $P = 50$ N, $V = 0.06$ m/s

Table 5 Wear parameters of the coatings ($P = 50$ N, $V = 0.05$ m/s)

Coatings	Wear rate (mm^3/m)	Depth wear track (μm)
NiCrBSi flame sprayed	16.12	20.96
NiCrBSi flame sprayed and flame remelted	10.45	13.65
NiCrBSi flame sprayed and induction remelted	7.39	9.59

as the loads are increased (as shown in Fig. 7b). No significant differences are found between the two types of coatings. The wear rates of the NiCrBSi alloy coating remelted by induction and of the SAE52100 steel as a function of the loads at a sliding speed of 0.05 m/s and a sliding duration of 20 min are presented in Fig. 7c. The wear rates of the induction remelted coating are observed to increase with increasing applied load. The wear rate of the coating is lower than that of the SAE52100 steel as the control, which indicates that NiCrBSi alloy coating remelted by induction has good wear resistance.

The analysis of both induction and flame remelted coatings indicates that there can be abrasive wear mechanism, adhesive wear mechanism and fatigue wear mechanism during the sliding process. Abrasive wear mechanism may be caused by the steel ball and the coating debris. For different speed and loads, the worn surface morphologies of the induction and flame remelted coatings are shown in Figs. 8 and 9, respectively. Obvious differences are found in the worn surface topography resulting from the different remelting processes, which may be due to the changes in size and distribution of the hard phases. In low load and low sliding speed, the stress acting on the surface is small, so the temperature on the worn surface is low. In this case, the wear is mild because severe oxidation cannot occur; as a result, the hard phases act as hard barriers to resist the plastic deformation of the soft matrix (plastic deformed soft matrix against the hard phase, as shown in Fig. 8c). So under this condition, abrasive wear is relatively important mechanism. However, when the values of the load and sliding speed increases, both the stress and the temperature on the worn surface dramatically increases. High hardness asperities of the coatings can press and cut the counterpart steel, which will then lead to an adhesive layer on both the remelted coatings under a high sliding speed and load (as shown in Figs. 8b and 9b). It can be seen that adhesive wear mechanism causes material transfer. The fatigue wear mechanism can also have a relevant role because cracks are observed on worn surface of the flame remelted coating surface (as shown in Fig. 9c). Thus, these cracks may cause crater on the worn surface, which is the main reason for the increased wear rate of the flame remelted coatings under high load and a high sliding speed. Table 5 lists the wear

depth on both coatings. The values indicate that induction remelting process promotes the sliding wear resistance. The improvement in the wear resistance of the coatings remelted by induction can be attributed to the following: first, the small, round shape and uniformly distributed microstructure characteristics can increase the hardness of the coatings remelted by induction, which is beneficial for better wear resistance. Second, using the FEGSEM to perform further analysis of the hard phase distribution for the coatings remelted by induction may improve the wear resistance. Third, the well-distributed hard phases can act as a wear resistance skeleton, which can also contribute to the improvement of the wear resistance.

4 Conclusions

The appropriate selection of the induction remelting process parameters allows for high quality NiCrBSi alloy coatings to be obtained on a carbon steel substrate. The microstructure, microhardness and wear resistance of the coatings have been investigated by examining the coating that has been remelted by flame and induction. The following conclusions can be drawn:

1. NiCrBSi alloy coatings remelted by induction have a smaller and uniformly distributed microstructure.
2. The microhardness of the coatings remelted by the induction method is higher than that of the coatings remelted by flame because of the fine uniform distribution of the structures in the coatings.
3. The wear mechanisms of the coatings are abrasive wear mechanism, adhesive wear mechanism and fatigue wear mechanism. The induction remelted coatings exhibit higher wear resistance than that of the flame remelted coatings.

Acknowledgements This study was financially supported by the National Natural Science Foundation of China (No. 51361020 and 51365024).

References

1. Prchlik L, and Sampath S, *Wear* **262** (2007) 11.
2. Zhang Z, Liang B, and Guo H, *J Therm Spray Technol* **23** (2014) 1404.
3. Yuping W, Pinghua L, and Chenglin C, *Mater lett* **61** (2007) 1867.
4. Zhang Z, Liang B, and Guo H, *J Therm Spray Technol* **23** (2014) 725.
5. Miguel J M, Guilemany J M, and Vizcaino S, *Tribol Int* **36** (2003) 181.
6. Lin L, and Han K, *Surf Coat Technol* **106** (1998) 100.
7. Uozato S, Nakata K, and Ushio M, *Surf Coat Technol* **200** (2005) 2580.

8. Gonzalez R, Garcia M A, and Penuelas I, *Wear* **263** (2007) 619.
9. Zhang Z Y, Wang Z P, Liang B, and La P Q, *Tribol Int* **39** (2006) 971.
10. Zhang Z, Wang Z, Liang B, Dong H B, and Hainsworth S V, *Wear* **262** (2007) 562.
11. Zhang Z, Wang Z, and Liang B, *Tribol Lett* **37** (2010) 141.
12. Houdková Š, Smazalová E, and Vostřák M, *Surf Coat Technol* **253** (2014) 14.
13. Kim H J, Hwang S Y, and Lee C H, *Surf Coat Technol* **172** (2003) 262.
14. Sharma S P, Dwivedi D K, and Jain P K, *Wear* **467** (2009) 853.
15. Navas C, Colaço R, and de Damborenea J, *Surf Coat Technol* **200** (2006) 6854.
16. Gonzalez R, Cadenas M, and Fernandez R, *Wear* **262** (2007) 301.
17. [17] Li Q, Zhang D, and Lei T, *Surf Coat Technol* **137** (2001) 69.
18. [18] Hu G, Meng H, and Liu J, *Appl Surf Sci* **308** (2014) 363.
19. [19] Chang J H, Chang C P, Chou J M, Hsieh R I, and Lee J L, *Surf Coat Technol* **204** (2010) 3173.
20. [20] Brunelli K, Dabalà M, Dughiero F, and Magrini M, *Mater Chem Phys* **115** (2009) 467.
21. [21] Kim M H, Rhee K Y, Paik Y N, Hong J S, and Ham Y S, *Mater Sci Eng A* **485** (2008) 31.